Influence of spatial variations in the lower critical field on the equilibrium field penetration into superconductors

Nurit Avraham,[1] E. H. Brandt,[2] G. P. Mikitik,[2,3] Y. Myasoedov,[1] M. Rappaport,[1] E. Zeldov,[1] C. J. van der Beek,[4] M. Konczykowski,[4] and T. Tamegai[5]

[1]*Department of Condensed Matter Physics, The Weizmann Institute of Science, Rehovot 76100, Israel*

[2]*Max-Planck-Institut for Metallforschung, D-70506 Stuttgart, Germany*

[3]*B. Verkin Institute for Low Temperature Physics & Engineering, National Ukrainian Academy of Sciences, Kharkov 61103, Ukraine*

[4]*Laboratoire des Solides Irradies, CNRS UMR 7642 and CEA-CMS-DRECAM, Ecole Polytechnique, 91128 Palaiseau, France*

[5]*Department of Applied Physics, The University of Tokyo, Hongo, Bunkyo-ku, Tokyo 113-8656, Japan*

(Received 24 January 2008; published 26 June 2008)

The thermodynamic lower critical field H_{c1} in $Bi_2Sr_2CaCu_2O_{8+y}$ crystals, in the presence of columnar defects, was determined using magneto-optical measurements combined with the shaking technique. We observe a downward shift in H_{c1} due to columnar defects. Using partially irradiated samples, we show that small local variations in H_{c1} dramatically affect the way the field penetrates into superconductors. We present a theoretical model which provides a quantitative fit to the experimental results and explains how the influence of small sample inhomogeneities is enhanced by geometrical effects and leads to significant variations in the local-field distribution and penetration.

DOI: 10.1103/PhysRevB.77.214525 PACS number(s): 74.25.Bt

I. INTRODUCTION

The thermodynamic lower critical field H_{c1} is one of the fundamental parameters of the mixed state in type II superconductors. At H_{c1} the formation of vortices becomes energetically favorable and the superconductor undergoes a transition from the Meissner state to the mixed state. The value of H_{c1} and the way the field penetrates into the sample are directly related to the free energy of a vortex and to essential mixed state parameters such as the penetration depth λ and the Ginzburg–Landau parameter κ. Experimentally, one measures the penetration field H_p, which differs from H_{c1} due to demagnetization effects which cause distortion of the external field. Due to this distortion the local field at the sample edges can be significantly higher than the applied field H_a and therefore field penetration occurs at H_p which is substantially smaller than H_{c1}.

An additional major difficulty in determining H_{c1} and moreover in measuring small variations in H_{c1} are the energy barriers against vortex penetration and bulk pinning, which may significantly increase H_p and hinder the system from reaching thermodynamic equilibrium. A major contribution to the hysteresis comes from geometrical[1–3] and surface[4,5] barriers. The geometrical barrier arises from the competition between the inward Lorentz force due to the Meissner shielding currents and the outward force due to increase in vortex line energy. The surface barrier arises from the competition between the attraction of vortices to the sample's surface and the inward repulsion due to Meissner currents flowing at the surface. In addition, bulk pinning delays vortex penetration into the sample resulting in a Bean critical state. As a consequence of the edge barriers and pinning, the studies of the phase transition at H_{c1} must usually contend with irreversibility and hysteresis. Most of the previous investigations therefore focused on the thermally activated penetration of vortices through the energy barriers and the way the nonequilibrium H_p is influenced by dynamic effects and by different kinds of disorder.[6–11]

In the present study, we aim at obtaining the thermodynamic H_{c1} and to investigate how small variations in H_{c1} affect the way the field penetrates into superconductors. To overcome the nonequilibrium conditions hindering the detection of the thermodynamic behavior, we use the vortex shaking technique[12,13] in which an in-plane ac field is used to "shake" the vortices toward their equilibrium state. The in-plane ac field generates dissipation[14–16] in the sample that causes the persistent currents to relax completely. This enables measuring the equilibrium properties of the vortex matter even in the presence of strong pinning.[13,17]

In order to form controlled spatial variations in H_{c1}, we irradiated the samples to create columnar defects (CDs) in specific regions. The introduction of CDs is expected to decrease the free energy of a vortex line[18–21] and consequently to reduce H_{c1}.[22–25] CDs are very effective in pinning vortices when oriented along the field direction and are usually used to enhance pinning and critical currents.[26–29] Here, however, we use the CDs for the purpose of reducing H_{c1}. The unwanted hysteretic effects of pinning are then removed by shaking.

We used differential magneto-optical (DMO) measurements[30–32] combined with the shaking technique to study the equilibrium field penetration into $Bi_2Sr_2CaCu_2O_{8+y}$ (BSCCO) crystals containing small regions with CDs. We observe an unexpectedly large variation in H_p between the irradiated and pristine regions and a remarkably abrupt field penetration which leads to a paramagnetic local magnetization in the irradiated regions. We derive a theoretical model that explains how, in the presence of large demagnetization effects, a small variation in H_{c1} can lead to significantly larger variations in the local H_p. The model also accounts for the observed positive local magnetization and provides a quantitative fit to the experimental data.

II. EXPERIMENTAL DETAILS

The measurements were performed on several BSCCO crystals ($T_c \approx 90$ K) irradiated at GANIL by 1 GeV Pb ions.

 ©2008 The American Physical Society

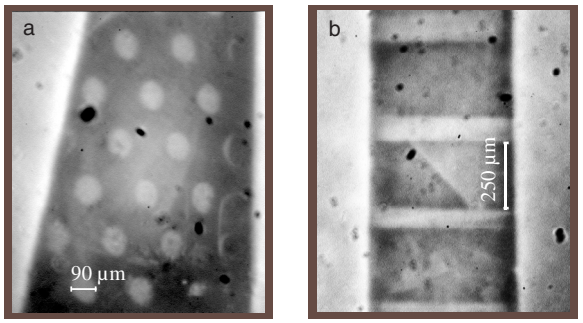

FIG. 1. (Color online) Magneto-optical images of crystals A and B in the presence of shaking. (a) Crystal A ($0.92\times1.5\times0.04$ mm^3 of trapezoidal shape) at $T=62$ K and $H_a=12$ Oe; the white circles show the enhanced flux in the irradiated regions. (b) Crystal B ($0.57\times1.2\times0.04$ mm^3) at $T=64$ K and $H_a=13$ Oe. The white horizontal strips are the irradiated regions.

The crystals were covered with masks prior to irradiation in order to produce the CDs, with density n_d equal to the ion dose, only in specific regions. This allows a sensitive comparison between irradiated and nonirradiated regions located in proximity to one another. The comparison between neighboring regions avoids possible differences in vortex behavior on larger scales arising from intrinsic inhomogeneities of the sample.[31,32] A dc magnetic field H_a was applied parallel to the crystalline c axis, while an ac transverse field H_{ac}, with frequency of 10 Hz and an amplitude up to 230 Oe, was applied along the a-b planes. The in-plane field generally reduces H_{c1}; however, in highly anisotropic materials such as BSCCO, the effect of the in-plane field is very small for our field values and is essentially the same in irradiated and pristine regions.[33,34] We measured several crystals, irradiated either along the c axis or at 45° with respect to the c axis. We present here results for two crystals irradiated through masks of different geometries: crystal A with matching field $B_\phi=n_d\Phi_0$ of 30 G, where Φ_0 is the flux quantum, was irradiated at 45° through a stainless-steel mask with a triangular array of 90 μm holes [Fig. 1(a)]. Crystal B, with $B_\phi=200$ G was irradiated parallel to the c axis, through a mask of gold strips, resulting in the formation of alternating irradiated and nonirradiated strips [Fig. 1(b)].

III. EXPERIMENTAL RESULTS

The suppression of the hysteresis by applying an in-plane ac field is demonstrated in Fig. 2 for both the pristine [Fig. 2(a)] and the irradiated [Fig. 2(b)] regions. The curves were extracted from a movie of conventional MO measurement by averaging over regions of 15×15 μm^2 each. Each figure shows two local magnetization loops B-H_a at 73 K with and without shaking. The curves were obtained using conventional magneto-optical measurements, in which a sequence of images is taken upon sweeping H_a. Without H_{ac}, a hysteretic behavior is observed in the pristine region and a larger hysteresis, due to enhanced pinning by CDs, is seen in the irradiated regions. Applying an ac field allowed us to suppress the hysteresis in both the pristine and the irradiated regions and to obtain fully reversible curves, as shown by the

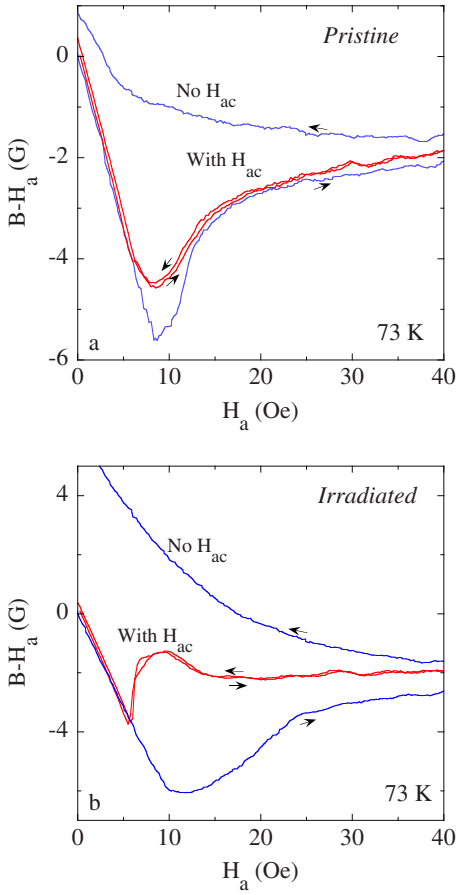

FIG. 2. (Color online) Local magnetization loops demonstrating the suppression of the hysteresis by an in-plane shaking field in crystal A in both the pristine and irradiated regions. The curves were measured while sweeping H_a in steps of 0.25 Oe. (a) Local magnetization loops with H_{ac} (red) and without H_{ac} (blue) measured in the pristine region. (b) Same as (a) for the irradiated regions.

red curves in Figs. 2(a) and 2(b). These reversible curves enable the determination of H_{c1} and the investigation of the transition from the Meissner state to the mixed state in equilibrium conditions.

Figure 3 presents a sequence of DMO images from a movie[35] of the transition from the Meissner state to the mixed state under equilibrium conditions upon sweeping H_a at 72 K. A DMO image is obtained by taking the difference between the MO images at $H_a+\delta H_a$ and $H_a-\delta H_a$ and averaging a large number of such differential images.[30] An abrupt change in the local density of the vortices appears as a bright feature in the DMO image. In Fig. 3(a) both the irradiated and the pristine regions are in the Meissner state, therefore, no change in the vortex density is detected upon field modulation and the whole sample appears dark. When increasing H_a to 6 Oe, a bright region appears in one of the irradiated regions in the left part of the sample, indicating a sharp penetration of vortices into the irradiated region. When further increasing the field, more vortices penetrate into this region, while the surrounding pristine regions are still in the Meissner state. In Figs. 3(d) and 3(e) the vortices penetrate into additional irradiated regions. Due to intrinsic inhomogeneity

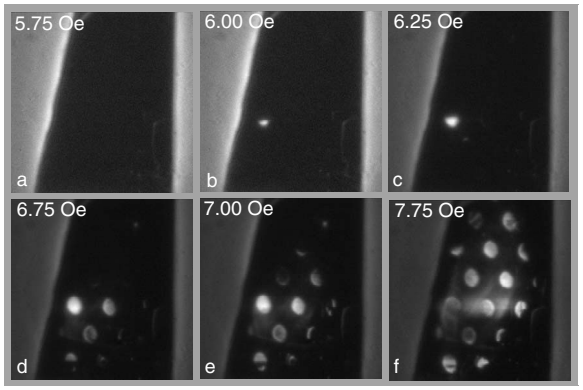

FIG. 3. A sequence of images from a movie of the transition from Meissner to mixed state in crystal A at 72 K in the presence of shaking. (a) At H_a=5.75 Oe, the sample is still in the Meissner state. (b) At 6 Oe, vortices start to penetrate into one of the irradiated regions. In (c), (d), and (e) the vortices penetrate into additional irradiated regions, but the pristine region is still mostly in the Meissner state. At 7.75 Oe the vortices penetrate also into the pristine region.

of the sample[31,32] and geometrical effects, however, the field does not penetrate simultaneously into all the irradiated regions. Yet it is clear that throughout the sample, the field penetrates first into the irradiated regions and only later into the adjacent pristine areas. Finally, at 7.75 Oe the vortices penetrate also into the pristine regions as shown by the bright region in the middle of the sample. Note that in crystal A the irradiated regions are surrounded completely by pristine region. Naturally, vortices are not expected to penetrate into the irradiated regions below H_{c1}^{pr} of the surrounding pristine region. However, due to the high anisotropy of BSCCO, Josephson vortices arising from the in-plane shaking field can penetrate the sample at vanishingly low fields. Consequently, vortices can accumulate in the irradiated regions once H_{c1} of the irradiated regions is exceeded.[36] We emphasize that all the essential findings were observed both in crystal A and in crystal B in which the vortices can penetrate directly into the irradiated regions [see Fig. 1(b)].

In order to compare the penetration of vortices into irradiated vs pristine regions, we plot, in Fig. 4(a), the equilibrium local magnetization curves for adjacent irradiated and pristine regions. The reduction in the penetration field H_p due to CDs is clearly shown. For a temperature of 68 K in crystal B, the penetration field of the irradiated regions H_p^{cd} is 2.8 Oe lower than H_p^{pr} of the pristine region. Another example is shown in Fig. 4(b) for crystal A at a temperature of 72 K. H_p^{cd} in the irradiated regions is 2.7 Oe lower than H_p^{pr} measured in the pristine region. To the best of our knowledge, this is the first unambiguous observation of reduction of H_{c1} by CDs.

The second important observation in Fig. 4(a) is the remarkable difference in the behavior of the magnetization in the irradiated and in the pristine regions near the penetration fields. In the pristine region, a gradual increase in flux density is observed when the penetration field $H_a=H_p^{pr}$ is exceeded. In contrast, in the irradiated regions, a sharp discontinuity in flux density appears at H_p^{cd} in both increasing and

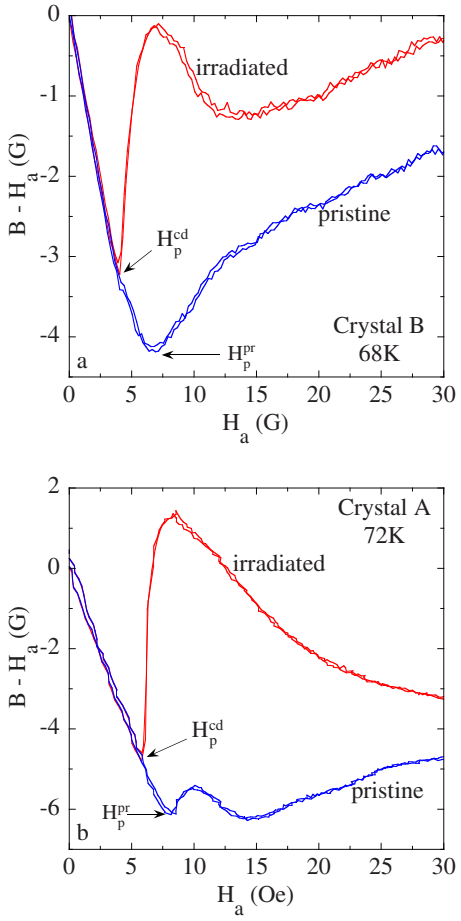

FIG. 4. (Color online) (a) Two reversible local magnetization loops measured in adjacent pristine (blue) and irradiated (red) regions, in crystal B, at 68 K in the presence of shaking. (b) Reversible local magnetization loops in crystal A at 72 K. The curves were measured while sweeping H_a in steps of 0.15 Oe. Note that in the irradiated region in (b), the local magnetization at the peak is positive.

decreasing branches of the magnetization curve. This is even more pronounced in Fig. 4(b) where the local magnetization in the irradiated regions increases abruptly from a negative value in the Meissner state to a positive value above penetration. This means that the induction B in the irradiated regions becomes larger than H_a. The sharp increase in B gives rise to the very bright signal seen in the DMO movies[35] and in Fig. 3. When further increasing H_a, the magnetization in the irradiated regions starts decreasing and eventually approaches the magnetization of the pristine region. We note that the curves are reversible and therefore describe the thermodynamic behavior of the system. The second dip observed around 14 Oe in the local magnetization of the pristine region in Fig. 4(b), apparently results from some inhomogeneity of the sample. This feature was not reproduced in other samples.

The field H_{c1} is related to the vortex line energy ε_l through the thermodynamic relation $H_{c1}=4\pi\varepsilon_l/\Phi_0$. It is favorable for the vortex core to be at the CD since this decreases its energy. For $r \ll \xi$, a vortex gains the condensation energy $\pi r^2 H_c^2/8\pi$ when residing on CD.[23,24,37] The line en-

ergies ε_l^{cd} and ε_l^{pr} and the lower critical fields H_{c1}^{cd} and H_{c1}^{pr} in the irradiated and pristine regions are then related through

$$\varepsilon_l^{cd} = \varepsilon_l^{pr} - \left(\frac{\Phi_0}{4\pi\lambda}\right)^2 \left(\frac{r}{2\xi}\right)^2, \tag{1}$$

$$H_{c1}^{cd} = H_{c1}^{pr} - \frac{\Phi_0}{4\pi\lambda^2}\left(\frac{r}{2\xi}\right)^2. \tag{2}$$

For the relative change in H_{c1}, we obtain

$$\frac{\Delta H_{c1}}{H_{c1}^{pr}} = \frac{H_{c1}^{pr} - H_{c1}^{cd}}{H_{c1}^{pr}} = \frac{(r/2\xi)^2}{\ln(\lambda/\xi)}. \tag{3}$$

For a temperature of 76 K, for example, using typical parameters for $YBa_2Cu_3O_7$ or BSCCO,[24] $\lambda_{ab}=1500/(1-T/T_c)^{1/2}$ Å, $\xi_{ab}=40/(1-T/T_c)^{1/2}$ Å, and $r=35$ Å for the radius of a CD, the relative change in H_{c1}, calculated by Eq. (3), is only ~0.8%. One would expect that the corresponding relative reduction in the penetration field would be of the same order of magnitude. In contrast, the measurements show that $\Delta H_p/H_p^{pr}$, at 76 K, is ~24%, much larger than $\Delta H_{c1}/H_{c1}^{pr}$. In addition, the penetration of vortices into the irradiated regions is remarkably more abrupt than the penetration into the pristine region.

IV. THEORETICAL MODEL

The above observations raise the question—how such small differences in H_{c1} can cause such large variations in field penetration? As we show below, the sharp penetration of vortices into the irradiated regions with an overshoot to positive local magnetization, as well as the significant variations in the penetration field, can be explained by a simple model describing the demagnetization effects in the pristine and the irradiated regions. We start by considering a long cylinder in a longitudinal field, where demagnetization effects are absent. We will continue with an ellipsoid in a perpendicular field where demagnetization effects are assumed to originate from the pristine matrix only. Then, we will generalize it to the case of an ellipsoid in a perpendicular field where demagnetization effects originate from both the pristine and irradiated regions.

Consider first a long cylinder in a longitudinal magnetic field H_a. In this geometry, demagnetization effects are absent, and the internal magnetic field H coincides with H_a. In this ideal case the induction may be calculated precisely using the Ginzburg–Landau (GL) theory,[38] and $B(H)$ exhibits infinite slope at $H_a=H_{c1}$ and tends to $B\approx H_a$ at $H_a \gg H_{c1}$. As shown previously,[38] $B(H)$ can be approximated by a simple model dependence,

$$B(H) = 0 \quad \text{for} \quad H \le H_{c1},$$

$$B(H) = (H^\alpha - H_{c1}^\alpha)^{1/\alpha} \quad \text{for} \quad H > H_{c1}, \tag{4}$$

which closely fits the exact GL solution. For the case $\kappa \gg 1$, the best fit is obtained when the value of the numerical parameter α is in the range of 2–3.[38] Although $B(H)$ in the irradiated and pristine materials are in general different,[25,39] we shall show below that our main experimental findings can be understood within the simplest approximation: the induction curves of the pristine and irradiated material exhibit the same $B(H)$ forms that differ only in their lower critical field values H_{c1}^{pr} and H_{c1}^{cd} in Eq. (4).

We now use these model $B(H)$ laws to calculate the inductions B^{pr} and B^{cd}, in the pristine and in the irradiated regions, when H_a is perpendicular to the platelet. We shall consider our specimens as ellipsoids with some demagnetization factor N $(0<N<1)$ and assume first that the irradiated regions do not affect the overall demagnetization effects. This approximation is well justified if the relative volume c of the irradiated part of the sample is small. Then, the internal magnetic field $H=H_a-4\pi NM(H)$ is obtained by solving the implicit equation,

$$H + N(B^{pr}(H) - H) = H_a, \tag{5}$$

where $B^{pr}(H)$ is the induction of the pristine material, and $M=(B^{pr}(H)-H)/4\pi$ is its magnetization. For an infinite platelet $(N=1)$, Eq. (5) gives $B=H_a$ and the penetration field $H_p^{pr}=0$. For a finite platelet, the internal field H in the region $H_a<H_p^{pr}$ is obtained from Eq. (5) by substituting $B^{pr}=0$. This yields

$$H = \frac{H_a}{1-N} \quad \text{for} \quad H_a \le H_p^{pr}. \tag{6}$$

The penetration fields for the irradiated and pristine regions are then given by

$$H_p^{pr} = (1-N)H_{c1}^{pr}, \tag{7}$$

$$H_p^{cd} = (1-N)H_{c1}^{cd}, \tag{8}$$

respectively. For $H_a>H_p^{pr}$, Eq. (5) can be solved numerically, but the sharpness of $B^{pr}(H)$ in the vicinity of $H=H_{c1}^{pr}$ means that $H\approx H_{c1}^{pr}$ if H_a does not exceed H_p too much. In this region of H_a (important for our experiments) Eq. (5) reduces to the form

$$B^{pr} \approx \frac{H_a - H_p^{pr}}{N} \quad \text{for} \quad H_a \gtrsim H_p^{pr}. \tag{9}$$

Note that in this approximation the H_a dependence of B^{pr} is *independent* of the explicit form of $B^{pr}(H)$. The internal field H at $H_a \gtrsim H_p^{pr}$ is found by substituting the model $B^{pr}(H)$, given by Eq. (4), into the left-hand side of Eq. (9). This yields

$$H \approx \left[(H_{c1}^{pr})^\alpha + \left(\frac{H_a - H_p^{pr}}{N}\right)^\alpha\right]^{1/\alpha} \quad \text{for} \quad H_a \gtrsim H_p^{pr}. \tag{10}$$

With this H, we get the induction $B^{cd}(H_a)$ in the irradiated regions,

$$B^{cd} = 0 \quad \text{for} \quad H_a \le H_p^{cd}, \tag{11}$$

$$B^{cd} = \left[\left(\frac{H_a}{1-N}\right)^\alpha - (H_{c1}^{cd})^\alpha\right]^{1/\alpha} \quad \text{for} \quad H_p^{cd} < H_a \le H_p^{pr}, \tag{12}$$

$$B^{cd} = \left[(H_{c1}^{pr})^{\alpha} + \left(\frac{H_a - H_p^{pr}}{N} \right)^{\alpha} - (H_{c1}^{cd})^{\alpha} \right]^{1/\alpha} \quad \text{for} \quad H_a \gtrsim H_p^{pr}, \tag{13}$$

Expansion of Eqs. (12) and (13) around H_p^{cd} and H_p^{pr}, respectively, shows that for $H_a \gtrsim H_p^{cd}$, $B^{cd} \propto (H_a - H_p^{cd})^{1/\alpha}$, while for $H_a \gtrsim H_p^{pr}$, $B^{cd} \propto (H_a - H_p^{pr})^{\alpha}$. This means that $B^{cd}(H_a)$ sharply increases in the narrow interval $H_p^{cd} < H_a < H_p^{pr}$, then it increases slowly. In contrast, $B^{pr}(H_a)$, grows approximately linearly with H_a, as shown by Eq. (9).

The above calculation explains the sharp penetration of the magnetic field into the irradiated regions. However, it provides a good approximation only if the total volume of the irradiated regions is much smaller than the platelet volume. In addition, this approach does not explain how a small variation in H_{c1} results in a large variation in H_p. Note that according to Eqs. (7) and (8) the relative change in H_{c1} and in H_p should be the same. In order to explain the experimental results and to allow the extraction of the lower critical fields, we now take into consideration the effect of the irradiated regions on the internal magnetic field H. Since this field is generated by a distribution of the magnetization over the whole sample, this effect can be approximately taken into account by a simple generalization of Eq. (5),

$$H + N[(1-c)(B^{pr} - H) + c(B^{cd} - H)] = H_a, \tag{14}$$

where c is the relative volume of the irradiated part of the sample. The penetration field H_p^{pr} is given by

$$H_p^{pr} = (1-N)H_{c1}^{pr} + cNB^{cd}(H_{c1}^{pr}). \tag{15}$$

This equation immediately follows from Eq. (14) for $H_a = H_p^{pr}$, $B^{pr} = 0$, and $H = H_{c1}^{pr}$. The penetration field H_p^{cd} is still defined by Eq. (8). The magnetic induction in the pristine region is approximately given by equations that are similar to Eq. (9) and that are valid unless $H_a \gg H_p^{pr}$,

$$B^{pr} = 0 \quad \text{for} \quad H_a \leq H_p^{pr}, \tag{16}$$

$$B^{pr} \approx \frac{H_a - H_p^{pr}}{N(1-c)} \quad \text{for} \quad H_a \gtrsim H_p^{pr}. \tag{17}$$

Note that both the penetration field H_p^{pr} and the slope of $B^{pr}(H_a)$ grow with c due to effective decrease in the demagnetization factor of the sample from N to $\sim N(1-c)$ caused by the initial flux penetration into the irradiated regions.

In the region $H_a \gtrsim H_p^{pr}$, H can be determined from Eqs. (17) and (4),

$$H \approx \left[(H_{c1}^{pr})^{\alpha} + \left(\frac{H_a - H_p^{pr}}{N(1-c)} \right)^{\alpha} \right]^{1/\alpha} \quad \text{for} \quad H_a \gtrsim H_p^{pr}, \tag{18}$$

while in the interval $H_p^{cd} \leq H_a \leq H_p^{pr}$ we use a linear interpolation of H between its values H_{c1}^{cd} and H_{c1}^{pr} at the ends of this interval. Then, B^{cd} is approximately described by the equations,

$$B^{cd} = 0 \quad \text{for} \quad H_a \leq H_p^{cd}, \tag{19}$$

$$B^{cd} \approx B^{cd}(H_{c1}^{pr}) \frac{H_a - H_p^{cd}}{H_p^{pr} - H_p^{cd}} \quad \text{for} \quad H_p^{cd} < H_a \leq H_p^{pr}, \tag{20}$$

$$B^{cd} = \left[(H_{c1}^{pr})^{\alpha} + \left(\frac{H_a - H_p^{pr}}{N(1-c)} \right)^{\alpha} - (H_{c1}^{cd})^{\alpha} \right]^{1/\alpha} \quad \text{for} \quad H_a \gtrsim H_p^{pr}, \tag{21}$$

that replace Eqs. (11)–(13). The inductions $B^{pr}(H_a)$ and $B^{cd}(H_a)$ were also calculated exactly numerically by solving Eq. (14) for the internal field H and inserting this H into the models $B^{pr}(H)$ and $B^{cd}(H)$. The approximate analytical expressions described above agree with the numerical calculations very well in the relevant region of $H_a \lesssim 2H_p^{pr}$.

The inclusion of the contribution from the irradiated regions can noticeably increase H_p^{pr}, as seen by comparing Eqs. (15) and (7). As we now show, this explains how, in agreement with our measurements, small spatial variations in H_{c1} are amplified and lead to a large spatial variations in the penetration field. This amplification can be shown by defining $H_{c1}^{cd} = (1-\epsilon)H_{c1}^{pr}$, where $0 < \epsilon \ll 1$, and writing the ratio between the relative changes in H_p and H_{c1} in terms of the sample parameters c, N, and ϵ. In order to simplify the expressions for the amplification in the following equations, we use $\alpha = 3$. From Eqs. (8) and (15) we hence obtain

$$\frac{\Delta H_{c1}}{H_{c1}^{pr}} = \epsilon, \tag{22}$$

$$\frac{\Delta H_p}{H_p^{pr}} = 1 - \frac{(1-N)(1-\epsilon)}{(1-N) + cN[1-(1-\epsilon)^3]^{1/3}} \approx \frac{3^{1/3}cN}{1-N}\epsilon^{1/3} + \epsilon, \tag{23}$$

and for the ratio, we obtain

$$\frac{\Delta H_p / H_p^{pr}}{\Delta H_{c1} / H_{c1}^{pr}} \approx \frac{3^{1/3}cN}{1-N}\epsilon^{-2/3} + 1. \tag{24}$$

This ratio, which measures the amplification, is always larger than 1. Moreover, it increases and finally diverges as $\epsilon \to 0$. Note that both ΔH_p and ΔH_{c1} remain finite and the divergence of the amplification arises from the fact that ΔH_p vanishes slower than ΔH_{c1}. The amplification factor is 1 for $c \to 0$ and it grows linearly with c. For $N = 0$, where demagnetization effects are absent, the amplification is also 1. This is inevitable since in this situation $H_p = H_{c1}$ in both the irradiated and pristine regions. Upon increasing N, the amplification diverges as $N \to 1$. We note that this amplification provides a tool to detect very small variations in H_{c1}.

To get a better understanding of this amplification we plot, in Fig. 5, the internal field H as a function of H_a. Initially, in the Meissner state, H increases linearly with a slope of $1/(1-N)$. This large slope is the result of the demagnetization factor N which causes a large field enhancement at sample edges. In the absence of irradiated regions the fast increase in H is stopped when H reaches H_{c1}^{pr}, which occurs at $H_p^0 = (1-N)H_{c1}^{pr}$ as marked in the inset of Fig. 5. Above H_p^0 flux penetrates rapidly into a pristine sample and, as a result, dH/dH_a has essentially zero slope, as indicated by the dotted line in the inset. In samples with irradiated regions, in con-

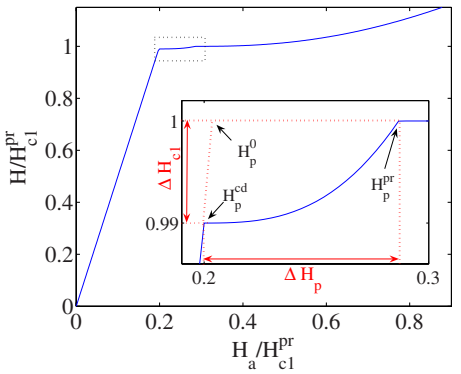

FIG. 5. (Color online) The internal field H vs H_a for $N=0.8$, $c=0.35$, and $\epsilon=0.01$. The inset shows a magnified view of the region $H_p^{cd}<H_a<H_p^{pr}$ (in units of H_{c1}^{pr}) marked by the dotted rectangle.

trast, the sharp flux penetration into these regions occurs at a reduced $H=H_{c1}^{cd}$. As a result the edge field is reduced sharply and any further increase in H is suppressed. The applied field H_a therefore has to be increased substantially before H can reach H_{c1}^{pr} that is required for penetration into the pristine regions, even though H_{c1}^{pr} is only slightly larger than H_{c1}^{cd}. This is the result of the vanishing slope of dH/dH_a above the first penetration, which implies that even a very small ΔH_{c1} results in a large ΔH_p increase in the penetration field of the pristine region. For parameters of Fig. 5, for example, $\Delta H_{c1}/H_{c1}^{pr}$ of 1% results in $\Delta H_p/H_p^0$ as large as 45%. Thus the effect of very small local variations in H_{c1} can be highly amplified and may lead to large variations in the equilibrium local penetration field.

The different effects of the sample geometry and the fraction of the irradiated area on the local magnetization are demonstrated in Fig. 6. The figure shows theoretical local magnetization curves $B-H_a$ for the pristine (solid) and irradiated (dashed) regions, plotted for different values of N and c. In Fig. 6(a) the curves are plotted for three values of N. The sharp penetration into the irradiated regions is clearly seen by the jump in the magnetization of the irradiated regions. Note that as N increases, H_p^{pr} and H_p^{cd} shift downward and the jump reaches higher values until, at $N=0.85$, it starts overshooting toward positive values, similar to the measured curves displayed in Fig. 4(b). In the opposite limit of $N\rightarrow 0$ the jump disappears and the magnetization curves of the irradiated and pristine regions show the same but shifted $B(H_a)$. In Fig. 6(b) we plot another set of theoretical curves, for different values of c. This figure clearly demonstrates the large effect of the irradiated regions on the penetration into the pristine regions. Upon increasing c from 0.05 to 0.4, H_p^{pr} shifts to higher fields while H_p^{cd} remains unaffected. This upward shift in H_p^{pr} is the amplification effect described by Eq. (24).

V. CORRESPONDENCE OF DATA AND MODEL

Figure 7 shows theoretical curves fitted to experimental data using the model $B(H)$. The solid lines are the measured local magnetization curves, obtained in crystal B, at 70 K,

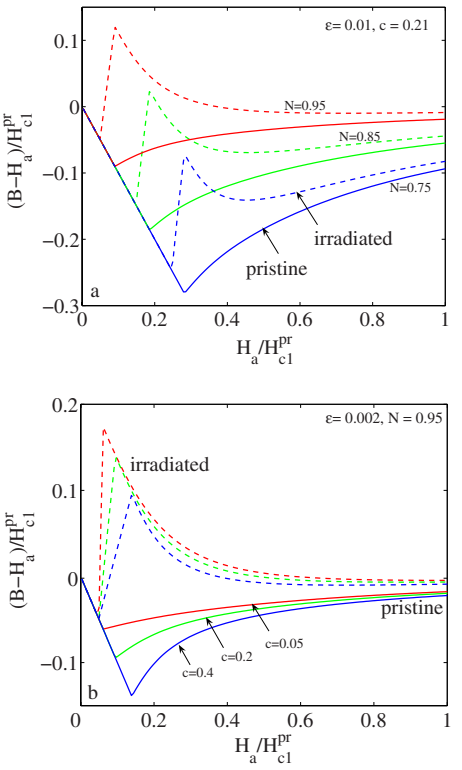

FIG. 6. (Color online) Theoretical local magnetization curves in the pristine (solid) and irradiated (dashed) regions plotted in units of H_{c1}^{pr}. (a) For $N=0.75$, 0.85, and 0.95. (b) For $c=0.05$, 0.2, and 0.4.

and the dashed lines are the theoretical fits. In the fit we used $c=0.35$, the actual measured fraction of the irradiated regions, and $H_p^{cd}=2.85$ Oe, as extracted from the experimental data. The best fit is obtained for $N=0.825$, $\epsilon=\Delta H_{c1}/H_{c1}^{pr}=0.04$, and $\alpha=2.4$. Apart from some deviations resulting due to inhomogeneities and the real shape of the sample, a very good agreement is observed, in particular, near H_p^{pr} and H_p^{cd}. This allows one to extract the thermodynamic lower critical fields. The present fit yields $H_{c1}^{cd}=16.28$ Oe and $H_{c1}^{pr}=16.95$ Oe. We note that the demagnetization factor resulting from the fit is in good agreement with our estimates of $N\sim 0.9$ obtained by approximating our samples as an ellipsoid with similar dimensions.

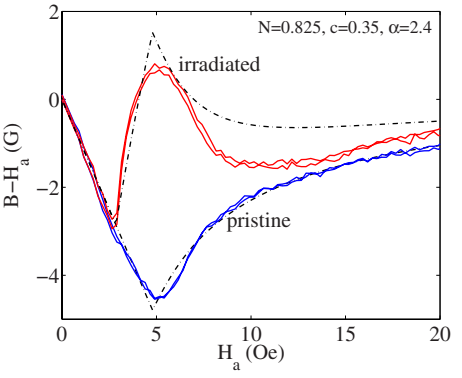

FIG. 7. (Color online) Theoretical local (dashed dotted) magnetization curves for the pristine and the irradiated regions, fitted to experimental curves (solid) obtained in crystal B at 70 K.

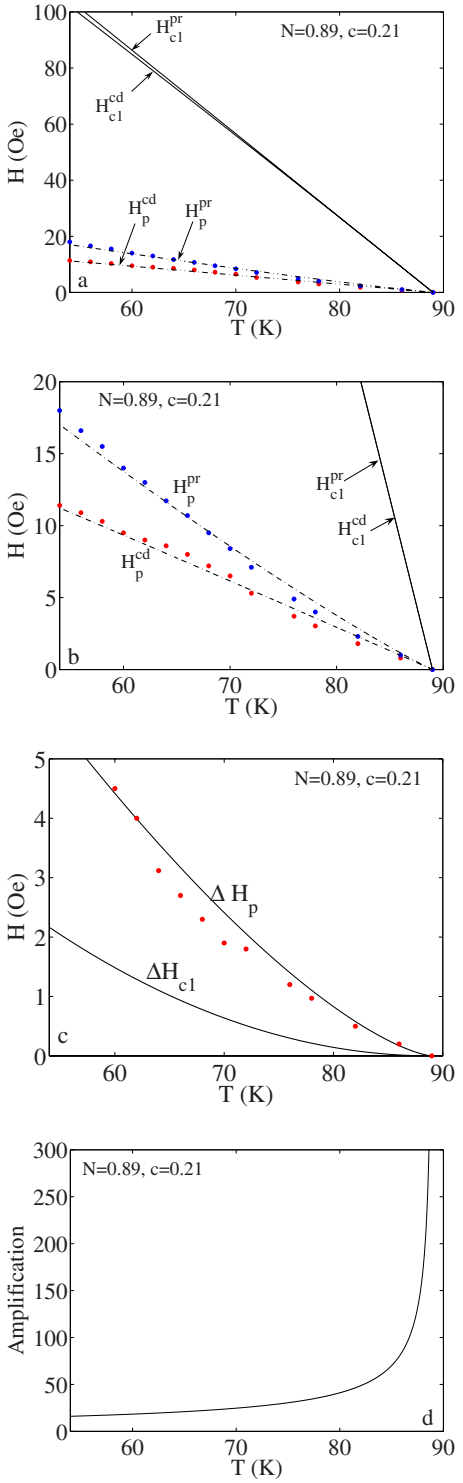

FIG. 8. (Color online) (a) Theoretical (dashed dotted) and experimental (solid symbols) $H_p^{pr}(T)$ and $H_p^{cd}(T)$ measured for sample A. The solid H_{c1}^{pr} and H_{c1}^{cd} are the theoretical estimates used to calculate the theoretical $H_p^{pr}(T)$ and $H_p^{cd}(T)$. (b) Magnified view of (a). (c) Theoretical (solid line) and experimental (solid symbols) $\Delta H_p(T)$ and ΔH_{c1} from (a). (d) The growth of the amplification factor Eq. (24) as ΔH_{c1} decreases with increasing temperature.

In Fig. 8(a) we plot the temperature dependence of $H_p^{pr}(T)$ and $H_p^{cd}(T)$ for crystal A in the temperature range above 55 K. Below this temperature, no reversible magnetization could be attained in this crystal with our maximum H_{ac}; hence, the equilibrium penetration fields could not be determined. The measured data are represented by the solid symbols and the calculated ones are shown by the dot-dashed lines. A very good fit is obtained. To calculate $H_p^{pr}(T)$ and $H_p^{cd}(T)$, we first estimated $H_{c1}^{pr}(T)$ and $H_{c1}^{cd}(T)$ from the vortex line energy [Eq. (2)] using, for example,[24] $\lambda_{ab}=1500/(1-T/T_c)^{1/2}$, $\xi_{ab}=40/(1-T/T_c)^{1/2}$ Å, and $r=35$ Å. Then we used our model [Eqs. (8) and (15)], with $\alpha=2.4$ and $c=0.21$, the relative irradiated volume in sample A, to calculate $H_p^{pr}(T)$ and $H_p^{cd}(T)$. The best fit is obtained for $N=0.89$. Figure 8(b) shows a magnified view of the fit between the theoretical and the experimental $H_p^{pr}(T)$ and $H_p^{cd}(T)$. In Fig. 8(c) we plot the calculated $\Delta H_{c1}(T)$ and the correspondence of the theoretical and measured $\Delta H_p(T)$. Note that at high temperatures, $\Delta H_{c1}(T)$ becomes very small and at above 85 K, it drops below 30 mOe, which would be below our experimental resolution. Yet, due to the amplification, $\Delta H_p \sim 300$ mOe, is still large enough to be detected. It turns out that such a geometry with strong demagnetization effects enables to detect small variations in H_{c1} down to about a few millioersted, which could not have been detected in the ideal longitudinal geometry. In Fig. 8(d) we plot the amplification factor as a function of temperature. Since ϵ, the relative change in H_{c1}, decreases with temperature due to the temperature dependence of λ and ξ, this figure demonstrates the increase in the amplification as ΔH_{c1} decreases by factors of more than 100.

VI. SUMMARY

In summary, we used magneto-optical measurements combined with the shaking technique to study the equilibrium field penetration into superconducting thin platelets containing small regions, in which CDs were introduced by heavy-ion irradiation. We observed reduction in H_{c1} due to CDs and a remarkably abrupt field penetration into the irradiated regions. We present a model that shows how geometrical effects can enhance small differences in the lower critical field and lead to large variations in the local penetration field. These phenomena should be very important in inhomogeneous samples—minute material inhomogeneities can significantly affect the way the field penetrates into the sample and can result in large variations in the local induction.

ACKNOWLEDGMENTS

We thank V. M. Vinokur and Ady Stern for stimulating discussions. This work was supported by the German Israeli Foundation (GIF), U.S.-Israel BSF, and Grant-in-aid from the Ministry of Education, Culture, Sport, Science, and Technology, Japan. E.H.B. and G.M. acknowledge the support by EU Transnational Access Program No. RITA-CT-2003-506095.

[1] M. V. Indenbom, G. D'Anna, M. O. Andre, V. V. Kabanov, and W. Benoit, Physica C **235-240**, 201 (1994).
[2] E. Zeldov, A. I. Larkin, V. B. Geshkenbein, M. Konczykowski, D. Majer, B. Khaykovich, V. M. Vinokur, and H. Shtrikman, Phys. Rev. Lett. **73**, 1428 (1994).
[3] M. V. Indenbom and E. H. Brandt, Phys. Rev. Lett. **73**, 1731 (1994).
[4] C. P. Bean and J. D. Livingston, Phys. Rev. Lett. **12**, 14 (1964).
[5] L. Burlachkov, A. E. Koshelev, and V. M. Vinokur, Phys. Rev. B **54**, 6750 (1996).
[6] M. Konczykowski, L. I. Burlachkov, Y. Yeshurun, and F. Holtzberg, Phys. Rev. B **43**, 13707 (1991).
[7] L. Burlachkov, Y. Yeshurun, M. Konczykowski, and F. Holtzberg, Phys. Rev. B **45**, 8193 (1992).
[8] M. Nideröst, R. Frassanito, M. Saalfrank, A. C. Mota, G. Blatter, V. N. Zavaritsky, T. W. Li, and P. H. Kes, Phys. Rev. Lett. **81**, 3231 (1998).
[9] J. K. Gregory, M. S. James, S. J. Bending, C. J. van der Beek, and M. Konczykowski, Phys. Rev. B **64**, 134517 (2001).
[10] A. E. Koshelev and V. M. Vinokur, Phys. Rev. B **64**, 134518 (2001).
[11] Y. M. Wang, A. Zettl, S. Ooi, and T. Tamegai, Phys. Rev. B **65**, 184506 (2002).
[12] M. Willemin, A. Schilling, H. Keller, C. Rossel, J. Hofer, U. Welp, W. K. Kwok, R. J. Olsson, and G. W. Crabtree, Phys. Rev. Lett. **81**, 4236 (1998).
[13] N. Avraham, B. Khaykovich, Y. Myasoedov, M. Rappaport, H. Shtrikman, D. E. Feldman, T. Tamegai, P. H. Kes, M. Li, M. Konczykowski, C. J. van der Beek, and E. Zeldov, Nature (London) **411**, 451 (2001).
[14] E. H. Brandt and G. P. Mikitik, Phys. Rev. Lett. **89**, 027002 (2002).
[15] G. P. Mikitik and E. H. Brandt, Phys. Rev. B **67**, 104511 (2003).
[16] G. P. Mikitik and E. H. Brandt, Phys. Rev. B **69**, 134521 (2004).
[17] H. Beidenkopf, N. Avraham, Y. Myasoedov, H. Shtrikman, E. Zeldov, B. Rosenstein, E. H. Brandt, and T. Tamegai, Phys. Rev. Lett. **95**, 257004 (2005).
[18] A. Wahl, V. Hardy, J. Provost, Ch. Simon, and A. Buzdin, Physica C **250**, 163 (1995).
[19] C. J. van der Beek, M. Konczykowski, T. W. Li, P. H. Kes, and W. Benoit, Phys. Rev. B **54**, R792 (1996).
[20] R. J. Drost, C. J. van der Beek, J. A. Heijn, M. Konczykowski, and P. H. Kes, Phys. Rev. B **58**, R615 (1998).
[21] C. J. van der Beek, M. Konczykowski, R. J. Drost, P. H. Kes, N. Chikumoto, and S. Bouffard, Phys. Rev. B **61**, 4259 (2000).
[22] G. S. Mkrtchyan and V. V. Shmidt, Sov. Phys. JETP **34**, 195 (1971).
[23] A. I. Buzdin, Phys. Rev. B **47**, 11416 (1993).
[24] G. Blatter, M. V. Feigel'man, V. B. Geshkenbein, A. I. Larkin, and V. M. Vinokur, Rev. Mod. Phys. **66**, 1125 (1994).
[25] R. A. Lehrer and D. R. Nelson, Physica C **331**, 317 (2000).
[26] D. R. Nelson and V. M. Vinokur, Phys. Rev. Lett. **68**, 2398 (1992).
[27] L. Civale, A. D. Marwick, T. K. Worthington, M. A. Kirk, J. R. Thompson, L. Krusin-Elbaum, Y. Sun, J. R. Clem, and F. Holtzberg, Phys. Rev. Lett. **67**, 648 (1991).
[28] M. Konczykowski, F. Rullier-Albenque, E. R. Yacoby, A. Shaulov, Y. Yeshurun, and P. Lejay, Phys. Rev. B **44**, 7167 (1991).
[29] C. J. van der Beek, M. Konczykowski, V. M. Vinokur, G. W. Crabtree, T. W. Li, and P. H. Kes, Phys. Rev. B **51**, 15492 (1995).
[30] A. Soibel, E. Zeldov, M. Rappaport, Y. Myasoedov, T. Tamegai, S. Ooi, M. Konczykowski, and V. B. Geshkenbein, Nature (London) **406**, 282 (2000).
[31] A. Soibel, Y. Myasoedov, M. L. Rappaport, T. Tamegai, S. S. Banerjee, and E. Zeldov, Phys. Rev. Lett. **87**, 167001 (2001).
[32] M. Yasugaki, M. Tokunaga, N. Kameda, and T. Tamegai, Phys. Rev. B **67**, 104504 (2003).
[33] N. Avraham, Y. Y. Goldschmidt, J. T. Liu, Y. Myasoedov, M. Rappaport, E. Zeldov, C. J. van der Beek, M. Konczykowski, and T. Tamegai, Phys. Rev. Lett. **99**, 087001 (2007).
[34] M. Konczykowski, C. J. van der Beek, A. E. Koshelev, V. Mosser, M. Dodgson, and P. H. Kes, Phys. Rev. Lett. **97**, 237005 (2006).
[35] See EPAPS Document No. E-PRBMDO-77-060821 for a movie of the transition from Meissner to mixed state at 72 K in the presence of shaking. For more information on EPAPS, see http://www.aip.org/pubservs/epaps.html.
[36] D. Cole, S. Bending, S. Savelev, A. Grigorenko, T. Tamegai, and F. Nori, Nat. Mater. **5**, 305 (2006).
[37] R. J. Drost, C. J. van der Beek, H. W. Zandbergen, M. Konczykowski, A. A. Menovsky, and P. H. Kes, Phys. Rev. B **59**, 13612 (1999).
[38] E. H. Brandt, Phys. Rev. B **68**, 054506 (2003); Physica C **404**, 74 (2004).
[39] A. I. Larkin and V. M. Vinokur, Phys. Rev. Lett. **75**, 4666 (1995).